A Dual-Mode Wi-Fi/BLE Wake-Up Receiver

Po-Han Peter Wang, *Member, IEEE*, and Patrick P. Mercier, *Senior Member, IEEE*

***Abstract*— This article presents a dual-mode wake-up receiver (WuRX) compatible with both Bluetooth-Low-Energy (BLE) and Wi-Fi transmitters. The proposed WuRX achieves the state-of-the-art power (as low as 4.4 μW through a latency-power duty-cycled tradeoff), sensitivity (as low as −92 dBm), and interference resilience (signal-to-interference ratio (SIR) = −67 dB) via a carefully architected frequency plan that supports BLE advertisement channel hopping or a proposed subcarrier-based within-channel Wi-Fi frequency hopping scheme, a carefully crafted frequency down-conversion plan that enables low-power receiver architecture via integer-*N* arithmetic, and an on-chip image rejection filter for full on-chip integration. The proposed design is implemented in a 65-nm CMOS process and operates from a 0.5-V supply.**

***Index Terms*— 2.4-GHz band, back-channel (BC) communication, Bluetooth Low Energy (BLE), frequency hopping, low-power wireless, wake-up radios, wake-up receivers (WuRXs), Wi-Fi.**

I. Introduction

THE energy consumed by small battery-powered devices used in applications, such as the Internet of Things (IoT), wearables, and smart homes, is often dominated by the embedded wireless radios. In applications with medium-to-low average throughput, a large fraction of this energy consumption typically comes from node-to-node network establishment requirements [1].

Since medium-to-low average throughput applications do not require continuous communication, a potentially impactful way to save energy is to keep the receiver in a low-power sleep state and only turn it on periodically after a predefined sleep timer expires. This duty-cycled receiver approach is shown in Fig. 1(a) and can be deployed both synchronously (e.g., in Wi-Fi) or pseudosynchronously [e.g., in Bluetooth Low Energy (BLE)] [2]. The effectiveness of this technique is dependent on the accuracy of the sleep timer—if it is not sufficiently accurate, then the receiver must turn on early to ensure that it guarantees successful capture of the packet and/or the transmitted packet must be repeated to guarantee proper reception. Since sleep timers have finite accuracies, this puts a lower bound on the realistically achievable duty cycle of the receiver. This is not a problem in medium-average-throughput applications where the duty cycle cannot be too low for throughput reasons but can significantly limit the energy consumption of low-average-throughput applications due to the need to constantly synchronize with the network even if no data need to be communicated.

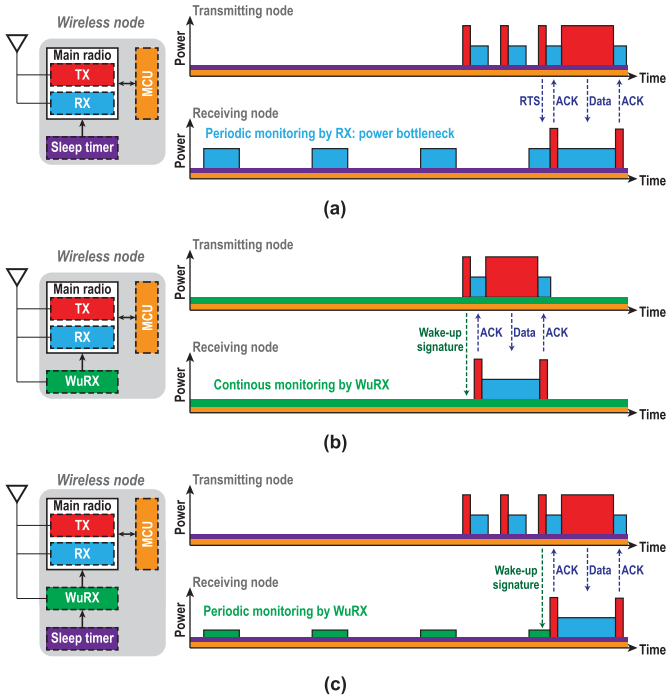

Fig. 1. Protocols to establish communication between wireless nodes. (a) Conventional duty-cycled main radio approach. (b) Always-ON WuRX approach. (c) Duty-cycled WuRX approach.

Instead of duty-cycling the main receiver, another approach to reduce energy consumption when continuous communication is not required is to employ an auxiliary always-ON wake-up receiver (WuRX) that continuously monitors the RF spectrum for a pre-defined wake-up signature. Once the wake-up signature is successfully received, as shown in Fig. 1(b), the main radio turns on to perform instantaneously high-speed (and power hungry) communication of one or more packets, after which it goes back into a sleep state until the next wake-up event. In order to impactfully reduce the overall energy burden of communication, the power consumption of the WuRX must be significantly lower than that of the main radio. Fundamentally, this requires trading off power consumption with one or more of modulation format and data rate (which set the spectral efficiency and wake-up latency), sensitivity, channelization, interference resiliency, or standards compliance [3]–[9].

Manuscript received August 23, 2020; revised November 13, 2020 and January 5, 2021; accepted January 8, 2021. Date of publication January 21, 2021; date of current version March 26, 2021. This article was approved by Guest Editor Brian Ginsburg. *(Corresponding author: Po-Han Peter Wang.)*

Po-Han Peter Wang was with the Department of Electrical and Computer Engineering, University of California at San Diego, La Jolla, CA 92093 USA. He is now with Broadcom Inc., San Diego, CA 92127 USA (e-mail: po-han-peter.wang@broadcom.com).

Patrick P. Mercier is with the Department of Electrical and Computer Engineering, University of California at San Diego, La Jolla, CA 92093 USA (e-mail: pmercier@ucsd.edu).

Color versions of one or more figures in this article are available at https://doi.org/10.1109/JSSC.2021.3051142.

Digital Object Identifier 10.1109/JSSC.2021.3051142

For pragmatic reasons, most of these items are not recommended to modify below the specifications of the main radio. For example, if the WuRX does not have as good of sensitivity as the main radio, then there is a mismatch between the achievable communication ranges of the two radios and existing network deployment strategies may have to undergo a costly redesign. Similarly, if the WuRX does not support the same standard as the main radio, then additional custom hardware is required on the transmitting node, which may be costly. Or, if the WuRX does not support similar channelization and interference resiliency compared to the main radio, then the WuRX simply will not be sufficiently robust in congested environments, limiting its usefulness in the same environments that the main radio is supposed to work in.

As a result, the main knob in which WuRXs reduce power compared to the main radio is in the data rate and the selection of the modulation format. In many low-average-throughput applications, a relatively long wake-up latency, for example, tens-to-hundreds of milliseconds or even up to 1 s, can be acceptable. How to achieve this in a manner that is compatible with existing standards will be discussed in Section II. Assuming for the moment that it is possible, achievement of the same sensitivity and interference resiliency as the main radio, even with relaxed data rate and modulation schemes, still requires significant power consumption [10]–[15].

To further reduce power, it is possible to combine the approaches in Fig. 1 (a) and (b) to create a duty-cycled WuRX, as shown in Fig. 1(c) [11]. For example, a prior-art Wi-Fi WuRX consumed 700 μW, which is high for a WuRX, but low for a radio with similar sensitivity and interference robustness compared to that of a full-fledged Wi-Fi receiver [15]. With careful design and duty-cycling, it is theoretically possible for this power consumption to be reduced by up to 70× or 3× if duty-cycled down to wake-up latencies of 10 ms to 1 s, respectively, for example. This can thus be an important knob to tradeoff between power and latency, iso other performance parameters.

In summary, a pragmatic and immediately deployable WuRX should feature sensitivity and interference resiliency as good as the main radio while consuming low power with or without duty-cycling and being compatible with the main radio it needs to work with. Since Wi-Fi and BLE are the two most popular radio standards for IoT, wearable, and smart home devices, a receiver that is compatible with both can potentially enable a wide range of new energy-constrained applications at low cost.

To this end, this article demonstrates a WuRX that is compatible with both Wi-Fi and BLE radios. The developed dual-mode WuRX achieves −92-/−90.3-dBm sensitivity with a latency-configurable power consumption of 4.4–352 μW, all while supporting multi-channel frequency diversity through a combination of a carefully architected frequency plan that supports BLE advertisement channel hopping or a proposed subcarrier-based within-channel Wi-Fi frequency hopping, a carefully crafted frequency down-conversion plan that enables low-power receiver architecture, and an on-chip image rejection filter for full on-chip integration. The proposed design was originally presented in [16]; this article provides significant additional wake-up signature and receiver architecture analysis, circuit implementation details, as well as additional measurement results. The proposed dual-mode frequency plan and enhanced 4-D wake-up signature is presented in Section II, while Section III describes the overall WuRX architecture. Section IV presents circuit implementation details, followed by measurement results in Section V. Finally, Section VI concludes this article.

II. Wi-Fi/BLE Standard-Compatible Wake-Up Signature

A. Overview of Prior-Art Wi-Fi/BLE Standard-Compatible Wake-Up Signatures

Wi-Fi and BLE both operate in the 2.4-GHz ISM band, which is a highly congested band with many devices operating simultaneously. Thus, good interference resiliency is a must when operating in this band. In part because of the need for high linearity and careful filtering and in part due to the complex and high data rate modulation schemes utilized in Wi-Fi and BLE, it is difficult for conventional receiver designs to operate at low (e.g., sub-mW) power levels while achieving good sensitivity. For example, Wi-Fi and BLE use modulation schemes such as 256-QAM orthogonal frequency-division multiplexing (OFDM) or frequency-hopped Gaussian frequency-shift keying (GFSK), which require complex demodulators with low phase noise local oscillators (LOs), filters, and/or digital signal processors. When coupled with high-linearity front ends and high data rates, achievement of low-power, especially at good sensitivity levels, is exceedingly difficult.

Since most low-power radios tend to utilize simple, low-complexity modulation schemes such as ON–OFF keying (OOK) or binary frequency-shift keying (BFSK) [1], a potentially effective way to reduce the power demands of a Wi-Fi or BLE-compatible WuRX is to make the otherwise complex modulation scheme look like a lower complexity scheme at a lower data rate. This concept, called back-channel communication, has enable many excellent low-power, yet standard-compatible receivers [4], [9]–[16].

1) Wi-Fi Compatible Back-Channel Wake-Up Signatures: As shown in Fig. 2(a), baseline Wi-Fi starting with IEEE 802.11g and onward communicates in one of three primary channels: 1, 6, and 11, located at 2412, 2437, and 2462 MHz, respectively. Each channel occupies 20 MHz of bandwidth during baseline operation. Within each channel, 52 OFDM subcarriers are enabled, and modulation ranging from BPSK to 256-QAM is embedded on each sub-carrier with a 4-μs symbol duration. To make this OFDM waveform appear to be lower complexity, prior work has suggested a multi-subcarrier OOK (MC-OOK) approach, where the middle 13 OFDM subcarriers (occupying ∼4 MHz of signal bandwidth) are turned on and off within a single 20-MHz Wi-Fi channel (within the standard-imposed peak-to-average power ratios) for OOK symbol 1 and symbol 0, respectively [11], [14], [15]. This method effectively reduces the receiving signal bandwidth and demodulation complexity, to the point where energy-detection architectures can be employed; this enables a low-power

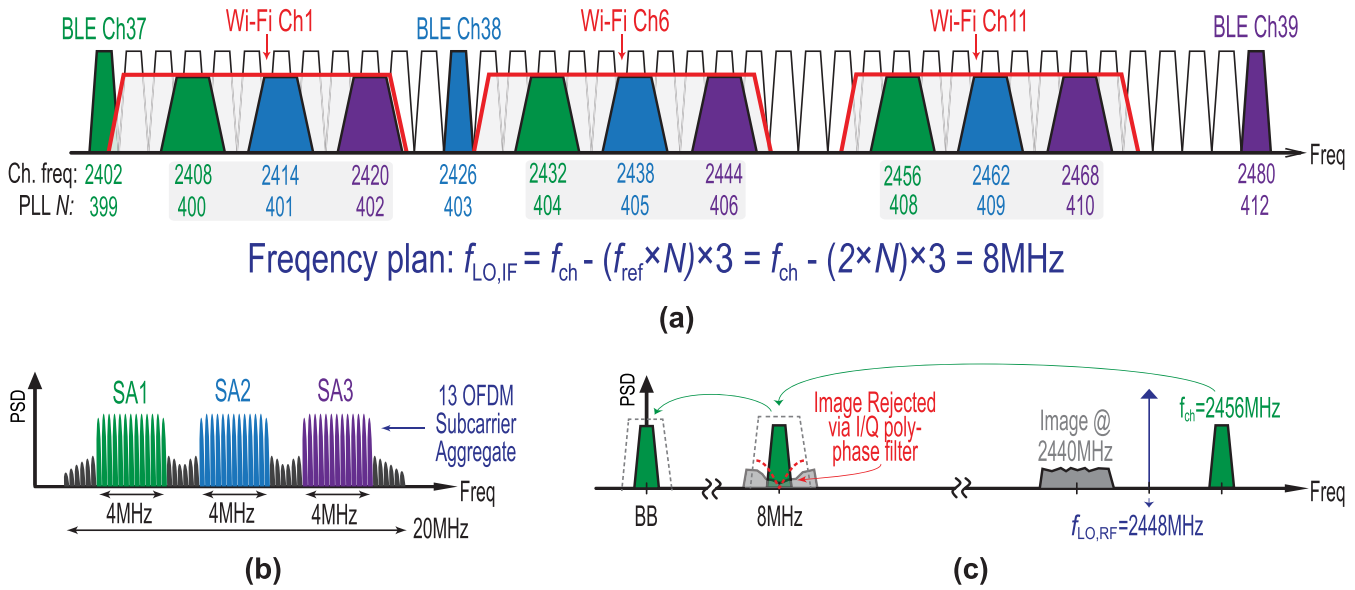

Fig. 2. (a) Proposed frequency plan for BLE/Wi-Fi dual-mode operation. (b) Proposed dynamic subcarrier aggregation for Wi-Fi mode. (c) Complete down-conversion flow using OFDM SA1 at Wi-Fi Ch. 11 as an example.

WuRX architecture. However, due to single-channel operation without frequency diversity, the achievable interference resilience relies solely on the linearity and filtering inside the WuRX itself, which may not be sufficient for truly robust operation at low-power levels.

2) BLE Compatible Back-Channel Wake-Up Signatures: As also shown in Fig. 2(a), BLE operates across 40 channels, with three of them (Ch. 37, 38, and 39 located at 2402, 2426, and 2480 MHz, respectively) dedicated for advertising events to establish node-to-node initial handshaking. The modulation for each channel is nominally GFSK at a 1-Mbps data rate. A single advertising event consists of three consecutively transmitted packets at each of the three advertising channels. A single advertising event takes less than 20 ms, and a single advertising packet length is between 128 and 376 μs.

Since the transmission of advertisement packets is required by the standard and the properties of the advertisement packets are well defined, most prior-art BLE-compatible WuRX performs OOK-like energy detection to detect the presence of either multiple advertising events [4], the RSSI and duration of a single channel packet [10], or the frequency hopping sequence [12], [13]. In particular, the work in [13] proposed a 4-D wake-up signature that looked at the RSSI, the packet duration, the inter-packet interval, and the frequency hopping pattern to improve coding diversity and interference resilience.

B. Proposed Dual-Mode Compatible Frequency Plan and Enhanced 4-D Wake-Up Signature

Although Wi-Fi and BLE operate with completely different modulation formats, it is possible to architect a back-channel modulation scheme that can use a similar frequency plan to enable reuse of underlying hardware. The overall plan is shown in Fig. 2(a). For BLE, the plan follows the same approach as in [13], where each of the three advertisement channels is down-converted in a time-sequenced manner to an 8-MHz IF via an LO generated by a 2-MHz reference integer-N phase-locked loop (PLL) followed by a frequency tripler. As abovementioned, the frequency-hopped nature of this approach imparts excellent interference resiliency for reception of BLE wake-up events in typical congested environments.

For Wi-Fi reception, one possibility is to use the same 4-MHz-wide MC-OOK signals as in prior work, so long as the selected sub-carriers are centered at a frequency compatible with the integer-N arithmetic of PLL used in the BLE mode. However, if a BLE (or any other type of) interferer is present nearby, the resulting Wi-Fi-compatible WuRX will not have any frequency diversity, and thus, the interference performance will be limited by the linearity and/or on-chip filter sharpness.

To include frequency diversity in a manner that is compatible with the integer-N-based BLE plan, this work proposes a dynamic subcarrier aggregation technique, shown in Fig. 2(b), which treats a group of 13 OFDM subcarriers as a subcarrier aggregate (SA), and this aggregate of 13 subcarriers hops between three different frequency locations within a single 20-MHz Wi-Fi channel. By carefully selecting the center frequency of each dynamic SA, which may not be the same relative subcarrier locations among all three Wi-Fi channels, the integer-N-based BLE frequency plan can be directly re-used for three Wi-Fi channels (1, 6, and 11) simply by using different values of N, as shown in Fig. 2(a). This enables dual-mode operation with the same underlying WuRX hardware all while supporting frequency diversity. The proposed dynamic SA-based back-channel modulation scheme can be enabled with commodity Wi-Fi hardware with a simple firmware modification. Note, however, that since the spacing between SA center frequencies is smaller in a single Wi-Fi channel than the spacing between BLE advertisement channels, the benefits of frequency diversity of the Wi-Fi mode are less than the benefits derived in the BLE mode. This will be seen in Section V.

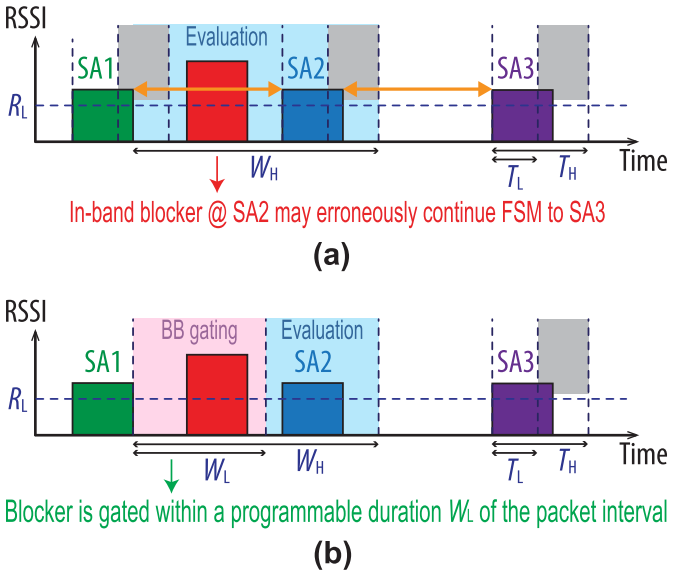

Fig. 3. 4-D wake-up signature with (a) evaluation period of the incoming packet covers the entire packet interval [13] and (b) proposed packet interval gating period for in-band blocker rejection enhancement.

Fig. 2(c) shows the down-conversion flow using SA1 at Wi-Fi Ch. 11 as an example. Here, SA1, which is located at 2456 MHz, is down-converted to an 8-MHz IF by an LO at 2448 MHz, generated from a 2-MHz reference multiplied by $N = 408$ and then again by the frequency tripler. Unlike [13], which required off-chip image rejection filtering, in this case, an IQ LO is generated, and the image is rejected fully on-chip via a passive IQ mixer followed by a polyphase filter, which will be described in more detail in Section III.

To further improve the interference resiliency for potential jammers that may occur in between BLE packets or dynamic SA transmissions, an enhanced 4-D wake-up detection scheme is proposed compared to [13]. Since the evaluation period of the incoming packet in [13] covers the entire packet interval to ensure no missed packets, an in-band blocker that occurs before the desired packet might incorrectly trigger the digital finite-state machine (FSM), as shown in Fig. 3(a). To solve this issue, this work proposes a packet interval gating logic technique that gates the digital baseband (BB) input to prevent blockers, which may show up right in the middle of the packet interval, from potentially initiating an erroneous state transition. Moreover, this gating window, W_L, is programmable based on the desired wake-up signature, as shown in Fig. 3(b).

III. Wake-Up Receiver Architecture

Based on whether or not a mixer is present, WuRXs can be loosely classified into direct energy detection architecture and mixer-based architecture [3]. As discussed in Section II, the proposed enhanced 4-D wake-up signature incorporates frequency hopping and therefore can potentially be applied to any mixer-based designs. However, to achieve low power and interference resiliency while being suitable for both BLE and Wi-Fi operation, it requires further considerations, which are discussed in this section.

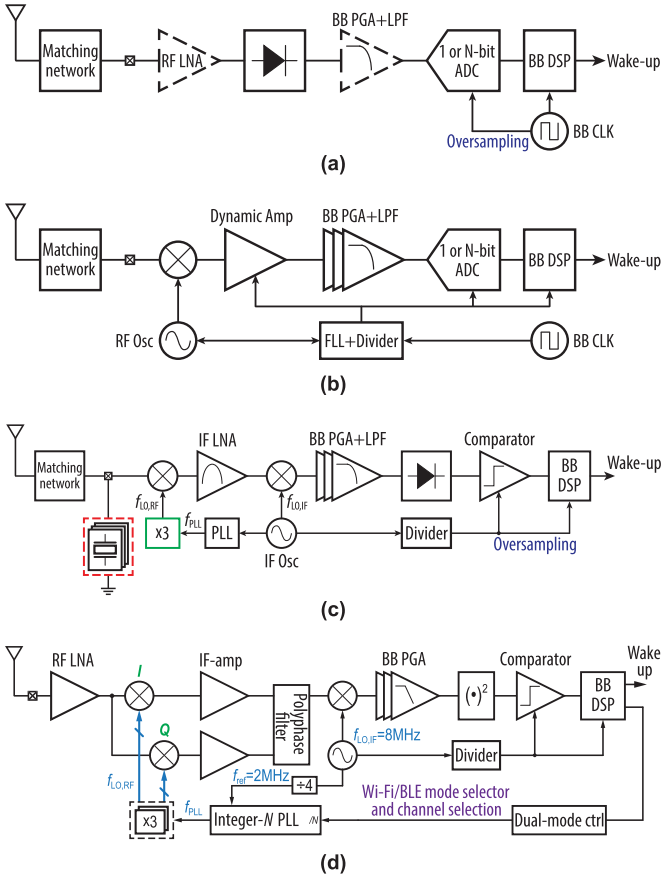

Fig. 4. Sub-mW standard-compatible WuRX architectures. (a) Direct envelope detection architecture [4], [9], [10]. (b) Mixer-first zero-IF architecture [11], [14], [15]. (c) Mixer-first heterodyne architecture [13]. (d) Proposed mixer-based zero second-IF heterodyne architecture with dual-mode control.

A. Overview of Standard-Compatible WuRX Architectures

1) Direct Energy Detection Architecture: The simplest possible back-channel-based modulation encodes information via the presence, or lack thereof, of packets (BLE) or SAs (Wi-Fi). Ignoring frequency hopping, the simplest possible receiver architecture is thus a simple direct energy detector, as shown in Fig. 4(a). Here, an envelope detector (ED) is used to directly down-convert RF signals to BB via a non-linear squaring function. Depending on sensitivity and power needs, an optional low-noise amplifier (LNA) can be included. If the LNA is not included, it is possible for this approach to reach the nW-to-μW level for general (i.e., not necessarily standard-compatible) WuRX applications [3]–[8]. However, wideband energy detection with limited pre-ED RF filtering implies limited channel selectivity, which causes any nearby interferers to also demodulate to BB. Moreover, since the ED's conversion gain depends on the square of its input voltage, the output signal-to-noise ratio is typically poor without sufficient pre-ED RF gain [17]. Thus, good sensitivity can only be achieved by burning power to increase pre-ED RF gain via one or more LNAs or by shrinking BB bandwidth to values well below what is possible by back-channel standard-compliant signaling.

For example, some of the nW-level WuRXs achieve sensitivities better than -80-dBm sensitivity but do so with a

very narrow BB bandwidths (e.g., 1–100 Hz) [7]. In contrast, energy detection of the longest possible BLE advertisement packet requires 376 μs, or a BB bandwidth greater than $\sim$3 kHz, with much higher bandwidth required for Wi-Fi, even with back-channel approaches. This increased noise bandwidth limits the sensitivities of such direct energy detecting architectures in prior standard-compatible 2.4-GHz WuRXs to -56.5 dBm at 236 nW [4] and -58 dBm at 164 μW [10] for BLE and -42.5 dBm at 2.8 μW [9] for Wi-Fi. On the other hand, recent work does show that by incorporating multistage RF LNAs, a sensitivity of -108 dBm can be achieved with a data rate of 4.2 kbps at 42 μW while achieving good SIR via a custom high-Q MEMS-based filter [18]. However, this work operates at 400 MHz and, therefore, requires substantially more power for a 2.4-GHz design. More importantly, the use of the MEMS filter limits the channelization, which is also in general a major downside of the direct energy detection architecture.

2) Mixer-Based Zero-IF Architecture: The two major downsides of the direct-ED approach relate to the lack of filtering at RF, which limits channel selectivity and interference resiliency, and the lack of pre-ED gain, which can only occur at power-expensive RF frequencies in this approach. To simultaneously address both of these issues, a mixer can be used to translate incident RF energy to a lower frequency, which is both easy and power efficient to filter and amplify the signal prior to energy detection. This, however, requires the generation of an LO, which must be accomplished through a PLL or a frequency-locked loop (FLL). Either way, the power of LO generation tends to dominate the power consumption of such approaches, placing them in a distinctly higher category than direct-ED-based approaches. Nevertheless, it is a necessary tradeoff to achieve the requisite selectivity, interference robustness, and sensitivity specifications at standard-compatible back-channel bandwidths.

Most prior-art Wi-Fi-compatible WuRXs utilize a mixer-first zero-IF architecture, as shown in Fig. 4(b) [11], [14], [15]. In this approach, the front-end RF LNA is removed to save power. Instead, the incident RF signal is, after an on-chip matching network, fed to a passive mixer, which down-converts the signal to BB for filtering and amplification. To achieve high sensitivity, low passive mixer switch resistance is required, which inevitably increases switch size and therefore passive mixer driver power. This further increases the LO generation and driving power requirement, especially given the 2.4-GHz frequency this occurs at.

Although this architecture does consume more power than a direct-ED approach, such receivers can still achieve sub-mW power and high sensitivity, with performance generally being better in a more scaled CMOS process where dynamic switching power is low. For example, in [11], a sensitivity of -72 dBm is achieved for 173 μW of power in 14-nm FinFET technology for Wi-Fi. However, since the signal bandwidth is purposely reduced for a WuRX, the sensitivity of this zero-IF approach is then limited by the post-mixer stage $1/f$ noise [11]. In [14], a dynamic amplifier with low $1/f$ noise is proposed to address this issue, which enables a design that achieves a sensitivity of -92.4 dBm under 340 μW of power in 28 nm, again for Wi-Fi.

Since the phase noise of the RF LO only needs to be around -80 dBc/Hz to not degrade the achievable sensitivity [19], ring oscillator-based LOs are typically employed, as they consume less power than an equivalent LC voltage-controlled oscillator (VCO). In addition, frequency synthesis can be accomplished via an FLL instead of a PLL to save power. Interestingly, however, phase noise still limits the SIR because of reciprocal mixing. Thus, further SIR improvements can be achieved by employing an LC oscillator as a tradeoff with power. For example, in [15], a sensitivity of -92.6 dBm with 16.6 dB better SIR compared to [14] is achieved under 495 μW of power in 28 nm for Wi-Fi. While this approach may work well for Wi-Fi back-channel communication, which has a larger signal bandwidth, careful re-design would be required when translating to lower bandwidths required by BLE to combat not only the more relatively important $1/f$ noise but also possible FLL frequency fluctuation, in order to properly demodulate the wake-up signal without sensitivity degradation.

3) Mixer-Based IF Heterodyne Architecture: To deal with $1/f$ noise issues that will come into play due to lower BLE bandwidths, a mixer-first heterodyne architecture can be adopted, which adds amplification at an IF away from the $1/f$ noise corner frequency [13]. This approach is shown in Fig. 4(c). The design in [13] achieves a sensitivity of -85 dBm for 220 μW of power in 65 nm in part by operating the RF LO at one-third of the signal frequency (with a frequency multiplier) and using a 0.5-V supply voltage. Moreover, a PLL instead of an FLL is adopted, which guarantees the frequency stability for low-bandwidth signal demodulation. It also achieves interference resiliency without the use of an LC oscillator when operating under the proposed three-channel frequency-hopping voting mode. However, without IQ RF LO signals, this prior art requires a custom off-chip single-die three-channel FBAR filter for image rejection. Although this off-chip image rejection approach is suitable for BLE applications that require a single FBAR die only, it cannot be operated under Wi-Fi mode without the use of multiple multi-channel FBAR die. For this reason, a new approach is needed to support dual-mode Wi-Fi/BLE operation.

B. Proposed Mixer-Based Zero Second IF WuRX Architecture

The proposed WuRX employs a mixer-based zero second-IF heterodyne architecture and is shown in Fig. 4(d). Before the first down-conversion, a matching network and current-reuse LNA provides 18 dB of RF gain, which provides sensitivity improvement over prior-art mixer-first architecture that has only $\sim$9 dB of passive voltage gain [13]. This comes at the cost of an additional 75 μW of power. After amplification, I/Q passive mixers are used to down-convert to the first IF at 8 MHz, where IF amplifiers can power-efficiently amplify the signal. A passive poly-phase filter can then be employed for image rejection without the need of an off-chip image rejection filter. After the second down-conversion, a programmable-gain BB amplifier with a built-in low-pass filter (LPF) further provides signal amplification and further rejects both noise and interferers to increase the ED output SNR. The ED then provides a squaring function for energy detection purposes.

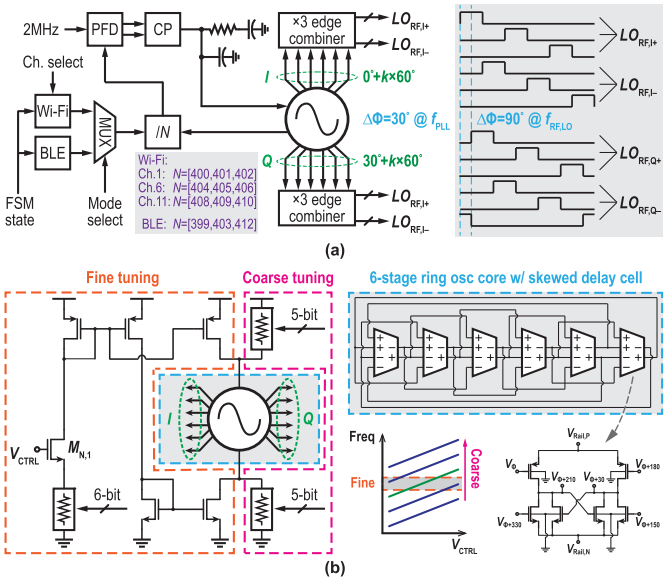

Fig. 5. Schematic of: (a) PLL with dual mode control logic and proposed IQ generation; (b) 6-stage 12-phase ring VCO with skewed delay cell and fine/course frequency tuning.

The ED's output is then oversampled and digitized by the comparator, which serves as a 1-bit analog-to-digital converter (ADC). The digital BB finally determines the wake-up and, along with the BLE/Wi-Fi dual-mode control logic, controls the channel selection for the RF front end.

The IF LO is generated by an off-chip 8-MHz crystal reference and serves as a global clock. The RF PLL is locked to the IF LO and then is fed to a frequency tripler to generate the RF LO. As in [13], a ring VCO is adopted in this design to save power since further interference resiliency can be achieved via the proposed three-channel frequency-hopping voting mode compared to the single-channel mode where SIR is limited by the phase noise. Circuit details of all these blocks are discussed in detail in Section IV.

IV. Circuit Implementation

A. RF LO Generation

Based on the proposed frequency plan shown in Fig. 2, the LO is generated via an integer-N PLL. A standard type-II PLL is adopted, as shown in Fig. 5(a), where the BLE channel or Wi-Fi SA is selected by changing the divider ratio, which is controlled by a dual-mode control logic based on an FSM.

Since the receiver is performing non-coherent energy detection, good phase noise is not required for proper demodulation (though reasonably good phase noise is required to minimize reciprocal mixing issues), and thus, a ring oscillator can be employed as the VCO. As shown in Fig. 5(a), an ~800-MHz ring VCO is employed to save power, while the 2.4-GHz band LOs are generated via an AND-based frequency-tripling edge combiner, which is the same strategy adopted in [13]. Unlike [13], however, I/Q RF LO signals are generated here to enable the on-chip image rejection filter. To generate these I/Q LOs, two sets of six-phase clocks with 30° separation are required, which, after the frequency tripler, can result in the desired I/Q RF LO signals at 2.4 GHz with 90° phase separation, as shown in Fig. 5(a).

To generate the required two sets of six-phase clocks (i.e., 12 LO phases), one possibility is to design a 12-stage single-ended ring oscillator. However, this is challenging to do at 800 MHz at 0.5 V (selected for low power reasons) in the employed 65-nm process. Instead, a differential 6-stage ring oscillator with skewed delay cells is adopted, where the skew delay cells can effectively boost the achievable oscillating frequency under the 0.5-V supply [20]. The VCO and the delay cells are shown in Fig. 5(b). Here, the PMOS bodies in the skewed delay cells are grounded to improve conductance, thereby reducing transistor size and, thus, CV^2 power. Since the supply voltage is only 0.5 V, there are no issues with substrate diodes turning on. To ensure PLL stability, both coarse- and fine-tuning paths are used to control K_{VCO} to be 320 kHz/mV in this design while still maintaining a large frequency tuning range to overcome process, voltage and temperature (PVT) [13].

The PLL settling time is ~13.7 μs based on simulations, which is sufficient for the minimum 345-μs packet interval based on the BLE signal generation software available in most commercially available phones.

B. RF/Analog Signal Chain

The overall RF/analog signal chain is shown in Fig. 6. First, in order to effectively increase the WuRX sensitivity compared to [13], a high-gain LNA is employed before the passive mixer. This comes with a cost of 75 μW in (measured) power overhead. The employed LNA achieves a simulated gain of 18 dB and a noise figure (NF) of 4 dB by using feedback capacitor C_F instead of a resistive feedback component to realize the input matching [21] all while using a current-reuse architecture and moderate-inversion biasing to increase gain efficiency under the same current consumption.

After the LNA, the signal is then fed to the RF passive mixer. As part of the tripler and on-chip image rejection circuit, each I/Q RF LO drives a two-phase six-switch passive mixer, which down-converts the signal to the 8-MHz IF. The I/Q IF signals are then amplified separately, fed to a polyphase filter, and then summed to achieve image rejection. A first-order passive polyphase filter is adopted here since it consumes zero power while providing sufficient image rejection ratio (IRR), i.e., >20 dB even with a 10% resistor variation [22] to maintain the same SIR as what otherwise occurs at +16-MHz frequency offset when operating in single-channel mode. The IRR can be further improved by cascading more orders of polyphase filters, but at the expense of higher IF amplifier power in order to maintain the same sensitivity, which is not ideal for the purpose of WuRX. More importantly, the SIR is not affected much by IRR if the frequency-hopping voting mode is enabled.

The IF mixer then down-converts the IF signal to BB. After this second down-conversion, in a similar manner to [13], a three-stage programmable-gain amplifier (PGA)/LPF provides gain in 3-dB steps as part of the power threshold setting to condition and filter the down-converted signal. In addition, a dc-offset cancellation loop is implemented to

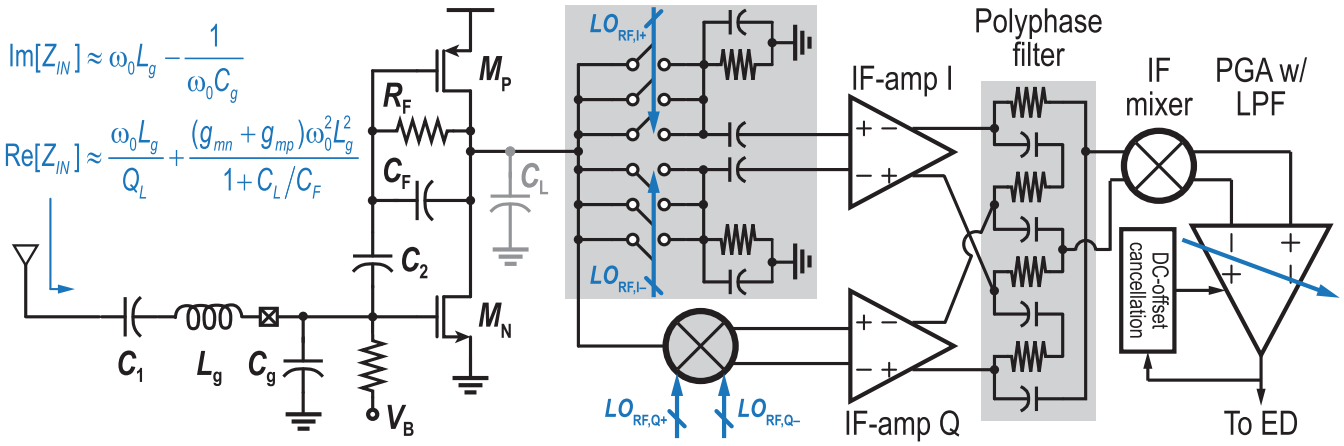

Fig. 6. Schematic of the WuRX signal chain.

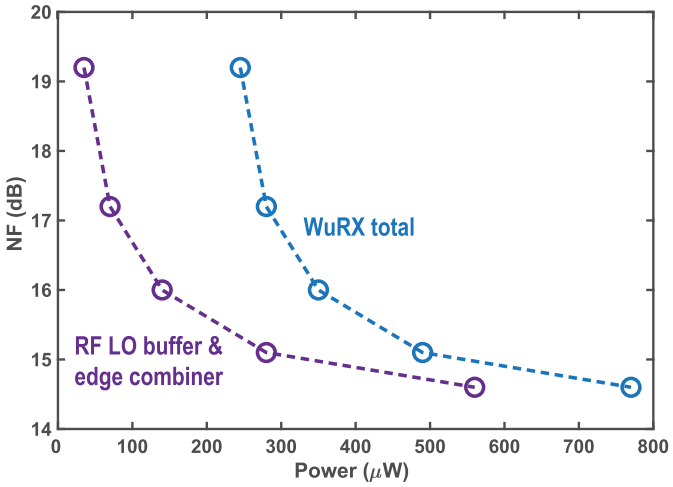

Fig. 7. Simulated WuRX NF versus power consumption for various passive mixer switch sizes.

prevent the three-stage PGA from being saturated by any dc-offset caused by mismatch, which avoids the use of large ac-coupling caps between each stage of the PGA. At high PGA gain settings, the WuRX sensitivity is limited by this pre-ED linear amplification portion of the signal chain, which has an NF of 16 dB based on simulations. Simulations show that 52% of the noise is from the RF passive mixer: a high ON-resistance value will degrade the NF, whereas a low-resistance value will enlarge the transistor size and therefore require a high power LO buffer to drive. Fig. 7 shows this tradeoff between power and noise, which suggests that if a more advanced process node is adopted (e.g., 28 nm in [14] and [15] or even 16 nm), this tradeoff can be much relaxed, while further sensitivity improvement can be achieved to match the state-of-art main receiver sensitivity (e.g., −95 dBm in [23] for BLE) under the same or even lower power budget.

C. Digital Baseband

Fig. 8 shows the block diagram of the on-chip digital BB, where an edge detector first compares the input signal

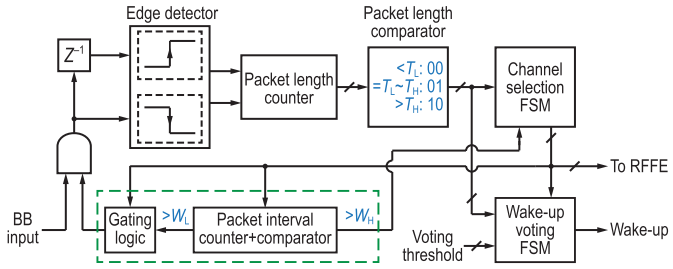

Fig. 8. Block diagram of the digital BB.

with a delayed version to extract the rising and falling edge timing of the packet (BLE) or dynamic SA (Wi-Fi), which are used to compute the packet/SA length. The measured packet/SA length is then compared to a pre-defined window, $T_{\mathrm{L}} \sim T_{\mathrm{H}}$, to generate a 2-bit control for the channel selection FSM and the wake-up voting FSM. The 2-bit state output of the channel selection FSM controls the RF front end to the desired channel/SA center frequency while providing the current sequencing order for the other blocks. Finally, the wake-up voting FSM generates the wake-up signal after three-channel scanning and comparison with a pre-defined voting threshold.

A packet interval computation is enabled after the first packet/SA is received and causes an FSM state change. If the packet interval is larger than an upper bound duration, W_{H}, and still no new packet is received, the FSMs rotate back to the initial stage. Unlike [13], where the entire between-packet interval is evaluated, here, an additional packet interval gating logic is implemented to gate out the digital BB for a programmable window, W_{L}, to prevent blockers that may occur right in the middle of the packet interval from potentially initiating an erroneous state transition, as discussed in Section II.

V. Measurement Results

The proposed dual-mode BLE/Wi-Fi WuRX is fabricated in a 65-nm process, occupying 0.6 mm^2 of core area. A die photograph is shown in Fig. 9.

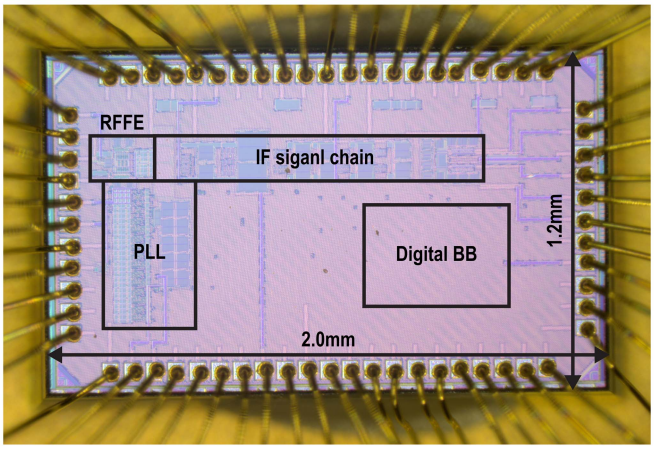

Fig. 9. Micrograph of the WuRX die.

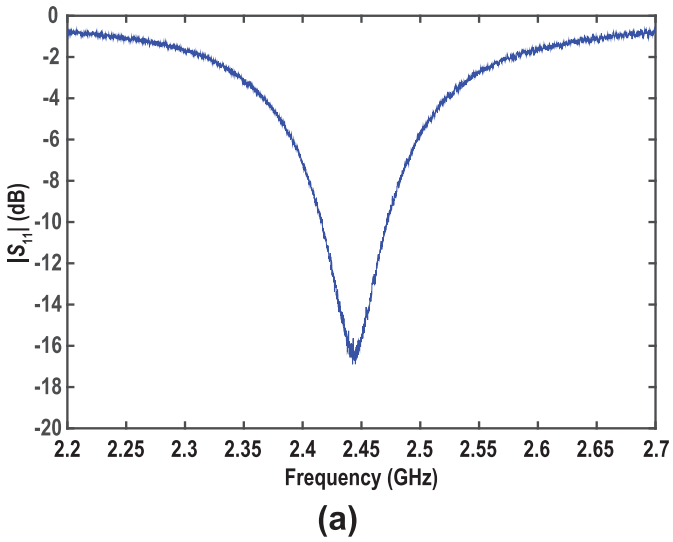

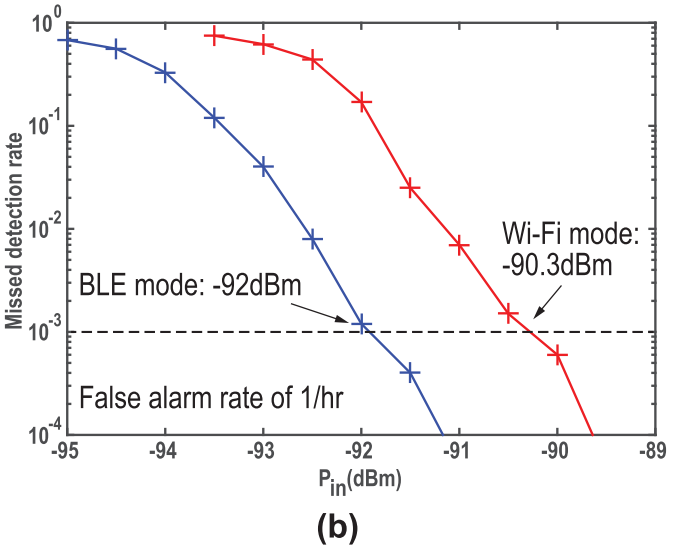

Fig. 10. Measurement results of (a) $|S_{11}|$ and (b) missed detection rate waterfall curve.

Fig. 10(a) shows the measured $|S_{11}|$, which demonstrates that the proposed WuRX is matched across the 2.4-GHz ISM band with $|S_{11}| < -8$ dB. This can be further improved by reducing Q of the LNA input tank slightly at the expense of a slightly degraded LNA NF since the WuRX sensitivity is more limited by the RF passive mixer switch, as discussed in Section IV.

The WuRX sensitivity is measured with random data transmissions (i.e., the incident data are not synchronized to the chip's clock) while monitoring missed detection at the output of the digital BB after the pre-defined wake-up signature is processed. Moreover, the digital BB is programmed to a voting threshold of three (i.e., all three signatures—packets in BLE or SAs in Wi-Fi—must be collected in order to trigger a wake-up event) in order to present sensitivity in the most aggressive false-alarm-avoidance setting. As shown in Fig. 10(b), the WuRX achieves a sensitivity of $-92/-90.3$ dBm for BLE/Wi-Fi modes, as measured by a missed detection rate of 10^{-3} under a false-alarm rate of <1/hr.

To verify the proposed WuRX performance with interference under practical operation, BLE-modulated jammers are used for SIR measurements, where the interferer power is defined as the power needed to achieve 0.1% MDR when the signal is 3 dB higher than at the nominal sensitivity point. When the WuRX is operating under a single-channel mode without the frequency-hopping voting scheme enabled, the on-chip image rejection and heterodyne structure enables an SIR of $-28.5/-21.7$ dB at 10-/24-MHz offsets, together with an image rejection of 22.5/17.5 dB for BLE/Wi-Fi modes. These measurements are shown in Fig. 11(a). When the frequency-hopping voting scheme is enabled, up to -67 dB SIR (limited by test equipment) is achieved for a normal short-burst jammer that corrupts one of the packets/SAs. This is shown by the green curve in Fig. 11(b). Moreover, for the extreme and much more rare case where a blocker exists throughout three-channel operation at just the right time intervals, the SIR is limited by the second most susceptible channel, as shown by the blue and red curves in 11(b) for BLE and Wi-Fi modes, respectively. It is also shown that under this extreme case, BLE mode has better SIR across band compared to Wi-Fi mode because of the larger frequency hopping channels separation. However, this is an exceptionally rare case and is unlikely to occur in practice except for intentionally nefarious jammers.

Fig. 12 shows the measured wireless transient waveforms of the WuRX operating in a realistic lab environment to demonstrate the effectiveness of the proposed wake-up signature processing algorithms. For the first experiment, shown in Fig. 12(a), the on-chip digital BB of the proposed WuRX is again programmed to a voting threshold of three like the sensitivity measurement in order to demonstrate the voting algorithm in the most aggressive false-alarm-avoidance setting. The first transmitted waveform has the expected three signatures with appropriate lengths and at appropriate inter-signature intervals, and thus, a wake-up event is generated. The second transmission in Fig. 12(a) utilizes a shorter inter-signature-interval than the receiver is programmed for. Due to the proposed input gating logic, most of the second signature's energy is not counted, which means that it

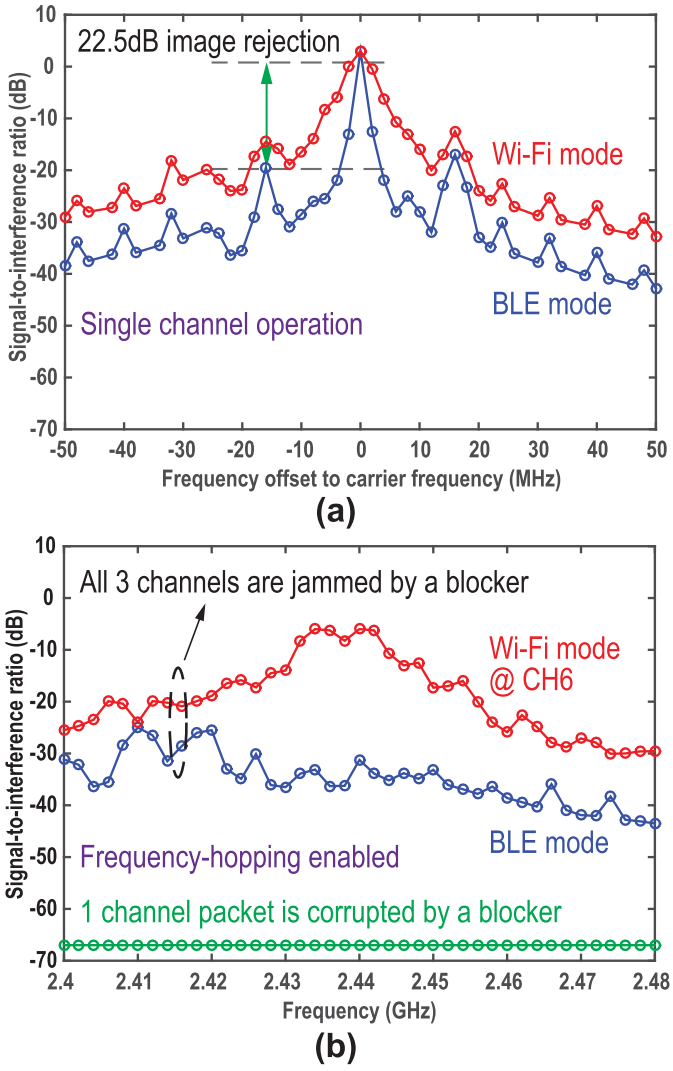

Fig. 11. Measurement results of SIR for all BLE adjacent channels within the 2.4 -GHz ISM band. (a) Without frequency hopping enabled. (b) With frequency hopping enabled.

TABLE I
POWER BREAKDOWN OF THE PROPOSED WURX

LNA	IF AMP	IF PGA	Comparator	Digital baseband	RF LO generation
76.5 μW	36.9 μW	21.7 μW	2.2 μW	3.8 μW	211.2 μW

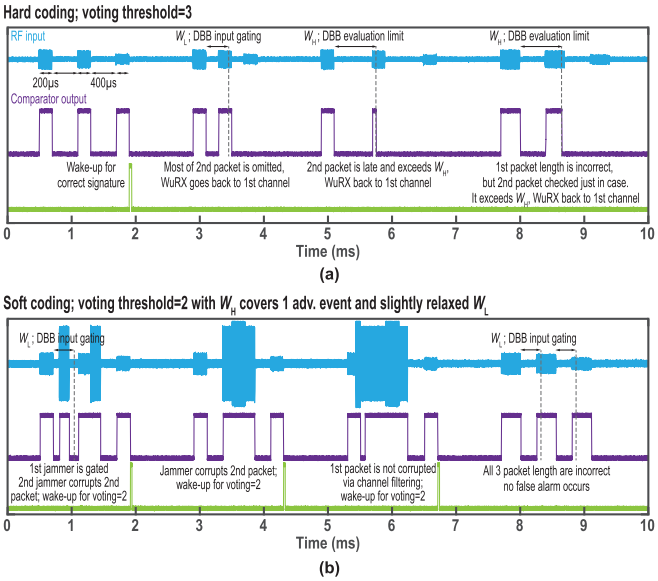

Fig. 12. Measured transient waveforms under wireless operation in a realistic lab setting for (a) different signatures under hard coding and (b) interferers under soft coding.

does not trigger the FSM to move to the next frequency, and thus, instead, the FSM reverts back to searching at the first frequency without a false alarm. The third transmission in Fig. 12(a) uses a longer inter-signature interval. Here, since the second packet comes in late and exceeds the packet evaluation limit, W_H, the WuRX also goes back to the first frequency and no false alarms occur. Finally, the fourth transmission in Fig. 12(a) uses a slightly longer signature length. Here, the receiver detects something at frequency 1, and although the signature length is incorrect, the WuRX will still move to the second frequency to scan just in case the first signature was correct but corrupted by jammers. However, since the second signature length in this example is also incorrect, no false alarms are generated.

For the second experiment, shown in Fig. 12(b), interfering Wi-Fi/BLE sources are placed right next to the receive antenna, and the on-chip digital BB of the proposed WuRX is programmed with a voting threshold of two to demonstrate that the proposed WuRX is interference-resilient while still being able to trigger correct wake-ups. In the first transmission, two in-band jammer packets are received simultaneously with the correct three signatures. Fortunately, the first jammer packet occurs within the digital BB gating window, and thus, it will not affect the wake-up signature processing algorithm. Although the second jammer packet occurs within the second wake-up signature period and therefore corrupts it, the first and third signatures are received correctly, and thus, a correct wake-up event is triggered due to the majority voting algorithm. Similarly, in the second transmission, a large and long jammer completely blocks the second signature; however, due to the majority voting algorithm, a correct wake-up event is generated. For the third transmission, where a longer jammer occurs across two wake-up signature periods, the built-in multistage filtering of the WuRX makes it such that only the second signature is corrupted, and thus, a correct wake-up event is still triggered. Finally, the fourth transmission again shows that a wrong wake-up signature, in this case with longer signature durations, will still not cause any false alarms under this majority voting setting because of the packet length counter.

Table I shows the power breakdown of the WuRX. During continuous operation, the WuRX consumes 352 μW, for a wake-up latency of 1.47 ms. Since 60% of the consumed power is in the LO generation, it is expected that the active mode power of this design can be significantly reduced by scaling to a smaller CMOS technology node. Importantly, however, by duty-cycling the WuRX via a power-gating

TABLE II
PERFORMANCE COMPARISON OF STATE-OF-THE-ART MIXER-BASED STANDARD-COMPATIBLE WURXS

	[11] JSSC'18	[12] JSSC'19		[13] ISSCC'19	[14] VLSI'19	[15] JSSC'20	**This Work**	
Wireless Standard	Wi-Fi	BLE		BLE	Wi-Fi	Wi-Fi	**Wi-Fi + BLE**	
Technology	14 nm	65 nm	45 nm	65 nm	28 nm	28 nm	**65 nm**	
Area	0.19 mm^2	1.1 mm^2	1 mm^2	1.3 mm^2	0.1 mm^2	0.18 mm^2	**0.6 mm^2**	
Supply Voltage	0.95 V	1.1 / 0.9 V	1.0 / 0.9 V	0.5 V	0.9 / 0.6 V	0.9 / 0.6 V	**0.5 V**	
Wake-Up Signature	Multi-subcarrier OOK	Frequency-hopped advertising channels		4-D signature with freq.-hopped advertising channels	Multi-subcarrier OOK	Multi-subcarrier OOK	**Wi-Fi Enhanced 4-D signature with freq.-hopped subcarrier aggregation**	**BLE Enhanced 4-D signature with freq.-hopped advertising channels**
RF LO Clock	Ring osc.	Ring osc.	LC osc.	Ring osc. + freq. tripler	Ring osc.	LC osc.	**Ring osc. + freq. tripler**	
LO Stabilization	XO + FLL	XO + FLL	None	XO + PLL	XO + FLL	XO + FLL	**XO + PLL**	
On-Chip Digital BB	Yes	No	Yes	Yes	Yes	Yes	**Yes**	
SIR	-20 dB @ 25 MHz	-4 / -11 dB @ 2 / 3 MHz	-10 / -15 dB[1] @ 2 / 3 MHz	-6 / -23 dB[2] @ 2 / 10 MHz -60 dB[3,4] across band	-32.4 dB @ 25 MHz	-49 dB @ 25 MHz	**Wi-Fi -21.7 dB[2] @ 24 MHz -67 dB[3,4] across band**	**BLE -12.5 dB[2] @ 2 MHz -67 dB[3,4] across band**
Total Power	173 μW	150 μW	1200 μW	220 μW	340 μW	495 μW	**4.4 μW[5] / 352 μW[6]**	
Wake-Up Latency and/or Bit Rate	62.5 kbps	1 ms / 112.5 kbps	1 ms / 250 kbps	200 μs[2] or 1.47 ms[3,7]	62.5 / 250 kbps	62.5 kbps	**1 s[3,5] or 1.47 ms[3,6,7]**	
Wake-up operation	Data bits	Data bits	Data bits	Wake-up only	Data bits	Data bits	**Wake-up only**	
Sensitivity	-72 dBm @ BER=10^{-3}	-57.5 dBm @ BER=10^{-3}	-82.2 dBm @ BER=10^{-3}	-85 dBm @ MDR=10^{-3}	-92.4 dBm @ PER=10^{-1}	-92.6 dBm @ PER=10^{-1}	**Wi-Fi -90.3 dBm @ MDR=10^{-3}**	**BLE -92 dBm @ MDR=10^{-3}**
False Alarms Rate @ Sensitivity	N.R.[8]	N.R.[8]	N.R.[8]	$<$2/hr	N.R.[8]	N.R.[8]	**$<$1/hr**	

[1] < -32 dB across band when frequency hopping is enabled.
[2] Single channel operation w/o frequency hopping mode enabled.
[3] 3-channel operation w/ frequency hopping mode enabled.
[4] Under the condition of 1 packet being jammed.
[5] WuRX in duty-cycle mode with 1.25% duty-cycle ratio.
[6] WuRX in always-on mode.
[7] BLE advertising event UUID=0x180D is used here for example.
[8] Not reported.

transistor, power can be traded off for wake-up latency, which is desirable in many emerging applications; measurements as low as 4.4 μW have been achieved for a wake-up latency of 1 s.

Table II show that the proposed WuRX achieves state-of-the-art sensitivity and SIR among BLE WuRXs, and comparable sensitivity and continuous-mode power to state-of-the-art Wi-Fi WuRXs, yet with improved SIR due to frequency hopping. In addition, it is the only dual-mode standard-compatible WuRX.

VI. CONCLUSION

This article presented a fully integrated dual-mode BLE/Wi-Fi WuRX that achieved -92/-90.3-dBm sensitivity at low, latency-configurable power consumption (4.4–352 μW) by: 1) exploiting frequency hopping, either via within-channel OFDM dynamic subcarrier aggregation (Wi-Fi) or via advertisement channels (BLE) to achieve interference resiliency; 2) carefully planning the location of OFDM SAs or BLE advertisement channels with integer-N arithmetic to enable a low-power IF down-conversion plan for both standards via an integer-N PLL; 3) employing a six-stage 12-phase skew-delayed ring oscillator that generates IQ LOs at low power while also enabling image rejection without an off-chip filter; 4) implementing a moderate-inversion current re-use LNA to improve sensitivity with a small power overhead; and 5) modifying the 4-D wake-up logic with packet interval gating to improve interference resiliency. Since the power consumption of the proposed design was dominated by the highly digital RF LO generation, implementation in an advanced process node can potentially further lower the power. Even at the current power level, especially with duty-cycling enabled, the power of the presented WuRX was measured to be significantly lower than conventional main radios, and yet, the WuRX could achieve similar sensitivity and interference resiliency as baseline Wi-Fi/BLE radios. As a result, the presented design could potentially help enable new wireless IoT applications, particularly those that have low average throughput requirements.

REFERENCES

[1] P. P. Mercier and A. P. Chandrakasan, *Ultra-Low-Power Short-Range Radios*. New York, NY, USA: Springer, 2015.
[2] E.-Y.-A. Lin, J. M. Rabaey, and A. Wolisz, "Power-efficient rendez-vous schemes for dense wireless sensor networks," in *Proc. IEEE Int. Conf. Commun.*, Jun. 2004, pp. 3769–3776.
[3] P.-H.-P. Wang *et al.*, "A near-zero-power wake-up receiver achieving –69-dBm sensitivity," *IEEE J. Solid-State Circuits*, vol. 53, no. 6, pp. 1640–1652, Jun. 2018.
[4] N. E. Roberts *et al.*, "A 236 nW -56.5 dBm sensitivity Bluetooth low-energy wakeup receiver with energy harvesting in 65 nm CMOS," in *IEEE ISSCC Dig. Tech. Papers*, Feb. 2016, pp. 450–451.

[5] P.-H.-P. Wang *et al.*, "A 400 MHz 4.5 nW –63.8 dBm sensitivity wake-up receiver employing an active pseudo-balun envelope detector," in *Proc. ESSCIRC 43rd IEEE Eur. Solid State Circuits Conf.*, Sep. 2017, pp. 35–38.
[6] J. Moody *et al.*, "Interference robust detector-first near-zero power wake-up receiver," *IEEE J. Solid-State Circuits*, vol. 54, no. 8, pp. 2149–2162, Aug. 2019.
[7] P.-H.-P. Wang *et al.*, "A 6.1-nW wake-up receiver achieving –80.5-dBm sensitivity via a passive pseudo-balun envelope detector," *IEEE Solid-State Circuits Lett.*, vol. 1, no. 5, pp. 134–137, May 2018.
[8] V. Mangal and P. R. Kinget, "A wake-up receiver with a multi-stage self-mixer and with enhanced sensitivity when using an interferer as local oscillator," *IEEE J. Solid-State Circuits*, vol. 54, no. 3, pp. 808–820, Mar. 2019.
[9] P.-H.-P. Wang, C. Zhang, H. Yang, D. Bharadia, and P. P. Mercier, "20.1 a 28μW IoT tag that can communicate with commodity WiFi transceivers via a single-side-band QPSK backscatter communication technique," in *IEEE Int. Solid-State Circuits Conf. (ISSCC) Dig. Tech. Papers*, Feb. 2020, pp. 312–314.
[10] M. Ding *et al.*, "A 2.4GHz BLE-compliant fully-integrated wakeup receiver for latency-critical IoT applications using a 2-dimensional wakeup pattern in 90nm CMOS," in *Proc. IEEE Radio Freq. Integr. Circuits Symp. (RFIC)*, Jun. 2017, pp. 168–171.
[11] E. Alpman *et al.*, "802.11g/n compliant fully integrated wake-up receiver with –72-dBm sensitivity in 14-nm FinFET CMOS," *IEEE J. Solid-State Circuits*, vol. 53, no. 5, pp. 1411–1422, May 2018.
[12] A. Alghaihab, Y. Shi, J. Breiholz, H.-S. Kim, B. H. Calhoun, and D. D. Wentzloff, "Enhanced interference rejection Bluetooth low-energy back-channel receiver with LO frequency hopping," *IEEE J. Solid-State Circuits*, vol. 54, no. 7, pp. 2019–2027, Jul. 2019.
[13] P.-H.-P. Wang and P. P. Mercier, "An interference-resilient BLE-compatible wake-up receiver employing single-die multi-channel FBAR-based filtering and a 4-D wake-up signature," *IEEE J. Solid-State Circuits*, early access, Aug. 12, 2020, doi: 10.1109/JSSC.2020.3012892.
[14] R. Dorrance *et al.*, "An ultra-low power, fully integrated wake-up receiver and digital baseband with all-digital impairment correction and −92.4dBm sensitivity for 802.11ba," in *Proc. Symp. VLSI Circuits*, Jun. 2019, pp. C80–C81.
[15] R. Liu *et al.*, "An 802.11ba-based wake-up radio receiver with Wi-Fi transceiver integration," *IEEE J. Solid-State Circuits*, vol. 55, no. 5, pp. 1151–1164, May 2020.
[16] P.-H.-P. Wang and P. P. Mercier, "A 4.4μW –92/–90.3dBm sensitivity dual-mode BLE/Wi-Fi wake-up receiver," in *Proc. IEEE Symp. VLSI Circuits*, Jun. 2020, pp. 1–2.
[17] X. Huang, G. Dolmans, H. de Groot, and J. R. Long, "Noise and sensitivity in RF envelope detection receivers," *IEEE Trans. Circuits Syst. II, Exp. Briefs*, vol. 60, no. 10, pp. 637–641, Oct. 2013.
[18] A. Dissanayake *et al.*, "A- 108dBm sensitivity, −28dB SIR, 130nW to 41μW, digitally reconfigurable bit-level duty-cycled wakeup and data receiver," in *Proc. IEEE Custom Integr. Circuits Conf. (CICC)*, Mar. 2020, pp. 1–4.
[19] A. M. Alghaihab, H.-S. Kim, and D. D. Wentzloff, "Analysis of circuit noise and non-ideal filtering impact on energy detection based ultra-low-power radios performance," *IEEE Trans. Circuits Syst. II, Exp. Briefs*, vol. 65, no. 12, pp. 1924–1928, Dec. 2018.
[20] C.-H. Park and B. Kim, "A low-noise, 900-MHz VCO in 0.6-μm CMOS," *IEEE J. Solid-State Circuits*, vol. 34, no. 5, pp. 586–591, May 1999.
[21] M. Silva-Pereira, J. T. de Sousa, J. Costa Freire, and J. Caldinhas Vaz, "A 1.7-mW –92-dBm sensitivity low-IF receiver in 0.13-μ m CMOS for Bluetooth LE applications," *IEEE Trans. Microw. Theory Techn.*, vol. 67, no. 1, pp. 332–346, Jan. 2019.
[22] B. Razavi, *RF Microelectronics*, 2nd ed. Upper Saddle River, NJ, USA: Prentice-Hall, 2011.
[23] M. Ding *et al.*, "A 0.8 V 0.8 mm^2 Bluetooth 5/BLE digital-intensive transceiver with a 2.3 mW phase-tracking RX utilizing a hybrid loop filter for interference resilience in 40nm CMOS," in *IEEE Int. Solid-State Circuits Conf. (ISSCC) Dig. Tech. Papers*, Feb. 2018, pp. 446–448.

Po-Han Peter Wang (Member, IEEE) received the B.S. degree in electrical engineering from National Taiwan University (NTU), Taipei, Taiwan, in 2011, and the M.S. and Ph.D. degrees in electrical and computer engineering from the University of California at San Diego (UCSD), La Jolla, CA, USA, in 2014 and 2019, respectively.

In 2013, he was an RFIC Design Intern with Broadcom Corporation, San Diego, CA, USA. He is currently an RFIC Design Engineer with Broadcom Inc., San Diego. His research interests include the design of energy-efficient transceiver for wireless communications, reconfigurable RF front ends and filters, and ultra-low-power mixed-signal circuits.

Patrick P. Mercier (Senior Member, IEEE) received the B.Sc. degree in electrical and computer engineering from the University of Alberta, Edmonton, AB, Canada, in 2006, and the M.S. and Ph.D. degrees in electrical engineering and computer science from the Massachusetts Institute of Technology (MIT), Cambridge, MA, USA, in 2008 and 2012, respectively.

He is currently an Associate Professor in electrical and computer engineering with the University of California at San Diego (UCSD), La Jolla, CA, USA, where he is also the Co-Director of the Center for Wearable Sensors. He was the Coeditor of *Ultra-Low-Power Short Range Radios* (Springer, 2015), *Power Management Integrated Circuits* (CRC Press, 2016), and *High-Density Electrocortical Neural Interfaces* (Academic Press, 2019). His research interests include the design of energy-efficient microsystems, focusing on the design of RF circuits, power converters, and sensor interfaces for miniaturized systems and biomedical applications.

Dr. Mercier received the Natural Sciences and Engineering Council of Canada (NSERC) Julie Payette Fellowship in 2006, the NSERC Postgraduate Scholarships in 2007 and 2009, the Intel Ph.D. Fellowship in 2009, the 2009 IEEE International Solid-State Circuits Conference (ISSCC) Jack Kilby Award for Outstanding Student Paper at ISSCC 2010, the Graduate Teaching Award in Electrical and Computer Engineering at UCSD in 2013, the Hellman Fellowship Award in 2014, the Beckman Young Investigator Award in 2015, the DARPA Young Faculty Award in 2015, the UC San Diego Academic Senate Distinguished Teaching Award in 2016, the Biocom Catalyst Award in 2017, the NSF CAREER Award in 2018, the National Academy of Engineering Frontiers of Engineering Lecture in 2019, and the San Diego County Engineering Council Outstanding Engineer Award in 2020. He has served as an Associate Editor for the IEEE TRANSACTIONS ON VERY LARGE SCALE INTEGRATION (TVLSI) from 2015 to 2017. Since 2013, he has served as an Associate Editor for the IEEE TRANSACTIONS ON BIOMEDICAL CIRCUITS AND SYSTEMS (TBioCAS). He is also a member of the ISSCC International Technical Program Committee, the CICC Technical Program Committee, and the VLSI Symposium Technical Program Committee and an Associate Editor of the IEEE SOLID-STATE CIRCUITS LETTERS.